JHEP

Published for SISSA by Springer

Received: July 4, 2014
Revised: July 28, 2014
Accepted: August 3, 2014
Published: August 26, 2014

JHEP08(2014)150

Topological susceptibility and the sampling of field space in $N_f = 2$ lattice QCD simulations

ALPHA Collaboration

Mattia Bruno, Stefan Schaefer and Rainer Sommer

John von Neumann Institute for Computing (NIC), DESY, Platanenallee 6, D-15738 Zeuthen, Germany

E-mail: mattia.bruno@desy.de, stefan.schaefer@desy.de, rainer.sommer@desy.de

Abstract: We present a measurement of the topological susceptibility in two flavor QCD. In this observable, large autocorrelations are present and also sizable cutoff effects have to be faced in the continuum extrapolation. Within the statistical accuracy of the computation, the result agrees with the expectation from leading order chiral perturbation theory.

Keywords: Lattice QCD, Lattice Gauge Field Theories

ArXiv ePrint: 1406.5363

doi:10.1007/JHEP08(2014)150

Contents

JHEP08(2014)150

1 Introduction

The topology of the gauge fields plays an important role in the understanding of the low energy structure of QCD. A prominent example is the Witten-Veneziano relation where the topological susceptibility of pure Yang-Mills theory is linked to the mass of the η' meson [1, 2]. The object of this paper is the topological susceptibility $\chi_{\rm top}$ in two flavor QCD, a quantity which vanishes in the chiral limit but whose value is non-zero for finite sea quark masses.

Precise measurements of $\chi_{\rm top}(m_\pi)$ are a challenge for the lattice. In particular significant effort went into finding a suitable definition of the topological charge on a discrete space time. Also large autocorrelations in the numerical simulations and sizable cutoff effects make the determination difficult.

These issues have a long history which we can only sketch briefly. The naive "field theoretical" definition of the topological charge density

$$q(x) = -\frac{1}{32\pi^2}\,\epsilon_{\mu\nu\rho\sigma}\,\mathrm{tr}\{F_{\mu\nu}(x)\,F_{\rho\sigma}(x)\}\,, \tag{1.1}$$

using some discretization of the field strength tensor F is known to lead to a topological susceptibility $\chi_{\rm top}$

$$\chi_{\rm top} = \frac{1}{V}\int dx \int dy\,\langle\, q(x)\,q(y)\,\rangle\,, \tag{1.2}$$

which suffers from non-integrable short-distance singularities. This has led to a vast array of operational procedures based on cooling and link smearing which remove the ultra-violet fluctuations of the gauge fields, but whose behavior towards the continuum limit is not well understood. However, a number of practical definitions with a well-defined continuum limit are now available, notably based on the properties of chiral Dirac operators and the index theorem [3] or ratios of certain fermionic correlation functions [4–6].

In this study, we adopt the definition of the topological charge through the Wilson flow [7], which provides a smoothing of the gauge fields with a smearing radius that is kept constant in physical units as the continuum is approached. Numerical support for a common continuum limit of this definition of the susceptibility and the method of refs. [4–6] in pure gauge theory has been given in ref. [8].

While the computation of the topological charge using the Wilson flow requires only a moderate numerical effort, the simulations are still expensive due to large autocorrelation times in the topological charge. In particular if periodic boundary conditions are adopted, the global topological charge suffers from a severe critical slowing down [9] and a determination of the susceptibility becomes practically impossible. The particularly poor scaling of the autocorrelation times due to the topological charge can be solved by using open boundary conditions in time [10, 11], however, the smooth fields in the construction of the topological charge are still slow in the Monte Carlo evolution.

Studying the effect of dynamical fermions on the susceptibility using lattice QCD has a long tradition, but even a decade ago, the situation was less than clear. While the Sesam collaboration did not find a convincing suppression of the susceptibility [12], the UKQCD collaboration did observe some effect [13]. Later, the importance of cut-off effects in this observable was discussed for simulations with Wilson fermions [14] and staggered quarks [15, 16]. After taking the continuum limit, a behavior compatible with the continuum expectation from Chiral Perturbation Theory [17] was found. More recently, the suppression of the susceptibility with the quark mass in two flavor QCD was also demonstrated in ref. [18] and [19] using Wilson fermions with a twisted mass and domain wall fermions, respectively.[1]

Due to the limitations by the statistical error and the discretization effects, the scope of this study is twofold: on the one hand, we want to present the measurement of $\chi_{\mathrm{top}}(m_\pi)$ as well as it can be made with currently available ensembles and present evidence for the proper suppression of the topological charge fluctuations with the quark mass. On the other hand, studying the autocorrelations in a set of gauge field configurations which are used in many computations serves as a crucial input in the error analysis of these computations [9]. We will also have a first look at the impact of open boundary conditions in time in simulations including dynamical fermions.

The paper is therefore organized as follows: in section 2 the observables are defined and an overview of the ensembles used in the current study is given. We examine the autocorrelations in observables constructed from smoothed gauge fields and give new estimates of the largest exponential autocorrelation times. In section 3, after the separation of the

[1] In ref. [18], there is a single lattice spacing for the 2-flavor results. For N_{f} =2+1+1 three lattice spacings are present but the continuum extrapolation assumes the susceptibility to vanish in the chiral limit at fixed lattice spacing, see our discussion in section 3.4.

JHEP08(2014)150

gauge fields into topological sectors is presented for the two flavor theory, we then turn to the computation of the susceptibility, the discussion of its discretization effects and a comparison of the continuum limit of $\chi_{\rm top}(m_\pi)$ with Chiral Perturbation Theory.

2 Setup of the calculation

The Wilson flow in the space of lattice gauge fields $U(x,\mu)$ is defined by the equations

$$\partial_t V_t(x,\mu) = -g_0^2\{\partial_{x,\mu} S_{\rm W}(V_t)\}V_t(x,\mu)\,, \quad V_t(x,\mu)\big|_{t=0} = U(x,\mu)\,, \tag{2.1}$$

where the action $S_{\rm W}$ is the standard Wilson action and V_t are the smoothed link variables at flow-time t. It was introduced in ref. [7] and we follow the conventions adopted there. In particular we will look at the topological charge density $q(x,t)$

$$q(x,t) = -\frac{1}{32\pi^2}\,\epsilon_{\mu\nu\rho\sigma}\,{\rm tr}\{G_{\mu\nu}(x,t)\,G_{\rho\sigma}(x,t)\}\,, \tag{2.2}$$

with a clover-type discretization of the field strength tensor $G_{\mu\nu}(x)$ constructed from links V_t. Furthermore the energy density constructed from these links will be considered

$$E(t) = -\frac{1}{2V}\sum_x {\rm tr}\{G_{\mu\nu}(x,t)\,G_{\mu\nu}(x,t)\}\,. \tag{2.3}$$

The quantities defined through the flow need to be evaluated at a fixed, physical value of t. Since it provides a smoothing of the fields over a radius $r=\sqrt{8t}$, it is natural to use the reference scale t_0 introduced in the original paper [7] through

$$t^2\langle E(t)\rangle\big|_{t=t_0} = 0.3\,. \tag{2.4}$$

Recently it has been argued that cutoff effects in some quantities can be reduced by considering the flow at a larger time t_1, where the right hand side of eq. (2.4) is replaced by $2/3$ [20]. We will give results in units of t_0 and t_1. To convert to physical units the reader may use $t_0 = 0.0236\,{\rm fm}^2$ [21] and $t_1 = 0.061\,{\rm fm}^2$, both obtained for $N_{\rm f}=2$ from fixing the kaon decay constant and the pion mass, m_π, to experiment. Their errors are negligible for our present purposes. While these numbers refer to the physical point, in the rest of this paper we always use the scales $t_0(m_\pi)$, $t_1(m_\pi)$ as obtained at the simulated values of m_π.

The topological susceptibility derived from the charge density eq. (2.2) does not require renormalization. While its continuum limit does not depend on the flow time t, discretization effects will be influenced by its choice. However, we will see below that choosing either $t=t_0$ or $t=t_1$ does not have a sizable effect on $a^4\chi_{\rm top}$.

Starting from the topological charge density defined in eq. (2.2), the topological charge can be directly obtained

$$Q(t) = a^4\sum_x q(x,t)\,. \tag{2.5}$$

In periodic boundary conditions, the susceptibility is then simply $\chi_{\rm top} = \langle Q^2\rangle/V$.

JHEP08(2014)150

β	ID	T/a	L/a	κ	m_π [MeV]	R	P_{acc}	MDU	stat/τ_{exp}
5.2	A2	64	32	0.13565	630	0.4	0.96	2953	76
	A3	64	32	0.13580	490	0.4	0.92	2965	76
	A4	64	32	0.13590	380	0.4	0.86	2989	76
	A5	64	32	0.13594	330	1.0	0.93	4004	102
	B6	96	48	0.13597	280	1.0	0.99	1272	33
	oB6	192	48	0.13597	280	1.0	0.85	1000	26
5.3	E5g	64	32	0.13625	430	0.4	0.84	5906	106
	F6	96	48	0.13635	310	0.4	0.88	1772	32
	F7	96	48	0.13638	260	0.4	0.86	3550	63
	G8	128	64	0.13642	190	1.0	0.99	1756	31
5.5	N6	96	48	0.13667	340	1.0	0.83	8040	74
	O7	128	64	0.13671	260	1.0	0.84	3920	36

Table 1. Overview of the ensembles used. We give the parameters of the action β and κ, the temporal and spatial extent of the lattice and the pion mass. For the simulations done with the DD-HMC algorithm, the ratio of active links, R, with which the τ_{int} are scaled throughout the paper, is below one. The last two columns give the total statistics in molecular dynamics units (MDU) and how this compares to the τ_{exp} estimated in eq. (2.9).

2.1 Ensembles

The set of ensembles used for our study was generated within the CLS effort.[2] Two degenerate light quarks have been simulated using O(a)-improved Wilson fermions and Wilson gauge action. The ensembles are listed in table 1: three lattice spacings $a \approx 0.075\,\text{fm}$, $0.065\,\text{fm}$, $0.048\,\text{fm}$ [22] and a range of pion masses are available with all lattices fulfilling $m_\pi L > 4$.

The majority of the ensembles was generated with the DD-HMC algorithm [23], while the HMC algorithm with Hasenbusch preconditioning [24] has been employed for those with smaller pion masses [25]. The ensemble where open boundary conditions in time have been imposed has been generated with the openQCD code [26]. The details of most of the simulations can be found in ref. [27].

Since a significant part of this text deals with autocorrelations, it should be noted that algorithms and their parameters influence them. The different ways the fermion determinants are treated in the three algorithmic setups will certainly matter once accuracies are high. At the current level of precision, we only correct for the inactive links during the trajectories of the DD-HMC algorithm by scaling the molecular dynamics time with R, the fraction of active links. In the high statistics pure gauge theory study of ref. [9] this has proven to correctly compensate for their effect. We will also scale autocorrelation times with the acceptance rate P_{acc} in the final scaling formula.

[2] https://twiki.cern.ch/twiki/bin/view/CLS/WebHome.

JHEP08(2014)150

2.2 Autocorrelations

Large autocorrelations are a well-known problem in lattice simulations. They are particularly pronounced in quantities constructed from the fields smoothed by the Wilson flow. In these quantities, a critical slowing down governed by a dynamical critical exponent of $z = 2$ is expected [28]. To compare simulations at different lattice spacings, we will therefore scale the Monte Carlo time with the dimension two quantity t_0 measured on the respective ensemble.

An additional problem is posed by the freezing of the topological charge as the continuum limit is approached. This occurs with a larger critical exponent — if it is not exponential — and makes simulation below $a \approx 0.05\,\mathrm{fm}$ exceedingly difficult. The problem is not restricted to the topological charge alone. In general, the associated slow eigenmodes of the Markov chain transition matrix contribute to the autocorrelation functions of all observables. For a correct estimate of the error a careful study of the slowest modes of the Markov chain is mandatory.

The basis of the error analysis of Markov Chain Monte Carlo data is the measurement of the normalized autocorrelation function ρ_A

$$\rho_A(\tau) = \frac{\Gamma_A(\tau)}{\Gamma_A(0)}\,; \qquad \Gamma_A(\tau) = \langle (A(\tau) - \bar{A})(A(0) - \bar{A}) \rangle\,, \tag{2.6}$$

with $A(\tau)$ the Monte Carlo time history of the observable A and τ the Monte Carlo time.

From the analysis of the spectral decomposition a recipe to include the coupling to the slow modes of the transition matrix in the error analysis has been given in ref. [9]: the normalized autocorrelation function ρ is summed as usual up to a window W and then the contribution of a single exponential with time constant τ_{exp} is attached

$$\tau_{\mathrm{int}} = \frac{1}{2} + \sum_{\tau=1}^{W-1} \rho(\tau) + \tau_{\mathrm{exp}} \rho(W)\,. \tag{2.7}$$

For this method an estimate of the largest time constant τ_{exp} in the simulation is needed. Since the dynamics of parity even and parity odd observables decouples [9], we can restrict ourselves to even ones. Then $Q^2(t)$ is an obvious candidate to look for the largest time constant, but we also investigate $E(t)$.

For the autocorrelation analysis we have to pick a value of the flow time t. In figure 1 we present the dependence of τ_{int} on this parameter and find a behavior similar to the one observed in pure gauge theory [26]: the data can be described by

$$\tau_{\mathrm{int}}(t) = c_0 + c_1 e^{-c_2 t}\,, \tag{2.8}$$

with the value at $t = t_0$ essentially capturing the asymptotic value. We therefore use this value of the flow time and drop the flow time argument in the following, using $Q = Q(t_0)$ and $E = E(t_0)$.

2.3 Results for autocorrelation times

Autocorrelation functions depend on the observable, the lattice spacing and the quark mass. To quantify the dependence on the physics parameters, we give examples of autocorrelation

JHEP08(2014)150

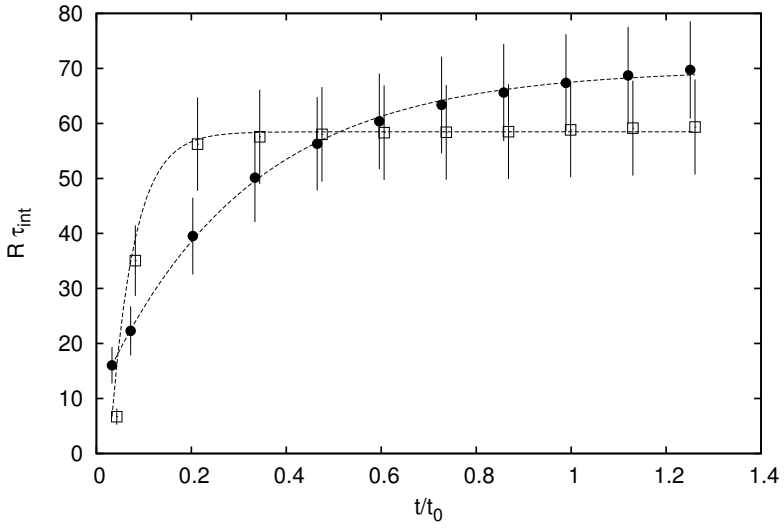

Figure 1. Integrated autocorrelation times of $Q(t)^2$ (open) and $E(t)$ (filled) from the ensemble N6, see table 1. Points have been shifted for better legibility. $\rho(\tau)$ is summed up to a window $W = 100\,\mathrm{MDU}$, neglecting a potential tail. The lines are fits of eq. (2.8) to the data with with $c_0 \approx 58\,\mathrm{MDU}$ for $Q(t)^2$ and $c_0 \approx 69\,\mathrm{MDU}$ for $E(t)$.

functions for two values of the quark mass in figure 2. The data at $\beta = 5.5$ shows a suppression with the quark mass of ρ_{Q^2}, as also found in ref. [29], whereas ρ_E is not affected beyond statistics. This can be understood from the fact that the topological susceptibility goes to zero in the chiral limit. The narrower distributions can be sampled in fewer steps leading to faster decorrelation in Monte Carlo time.

Figure 3 shows the dependence of the autocorrelation functions on the lattice spacing. While the rescaling of the Monte Carlo time with t_0 confirms the scaling properties of ρ_E already observed in pure gauge theory, the topological charge decorrelates much faster on the coarser lattices. On our finest lattice spacing, the autocorrelation functions of E and Q^2 are on top of each other and we expect the topological charge to dominate on finer lattices. This qualitative behavior is again similar to the one in pure gauge theory with periodic boundary conditions [10], only that it happens at smaller lattice spacing — not a surprise in light of the suppression of autocorrelations in Q^2 with the quark mass.

The results of the integrated autocorrelation times (summed up to $R\tau \approx 40 t_0/a^2$) for Q^2 and E are given in table 2. We also tried single exponential fits to the various ρ_E in order to find τ_{exp}, the largest time constant of the Monte Carlo chain. It turns out that the $\rho(\tau)$ are well described by this ansatz over essentially the full range of τ.

Since E has the largest autocorrelations in our range of lattice spacings and its autocorrelation function is approximately an exponential function, we can identify $\tau_{\mathrm{int}}(E)$ with τ_{exp} at the current level of accuracy. This leads to a parametrization valid for $\beta \in [5.2, 5.5]$

$$R\tau_{\mathrm{exp}}(\beta) = 11.3(1.8)\frac{t_0}{a^2}\,. \tag{2.9}$$

JHEP08(2014)150

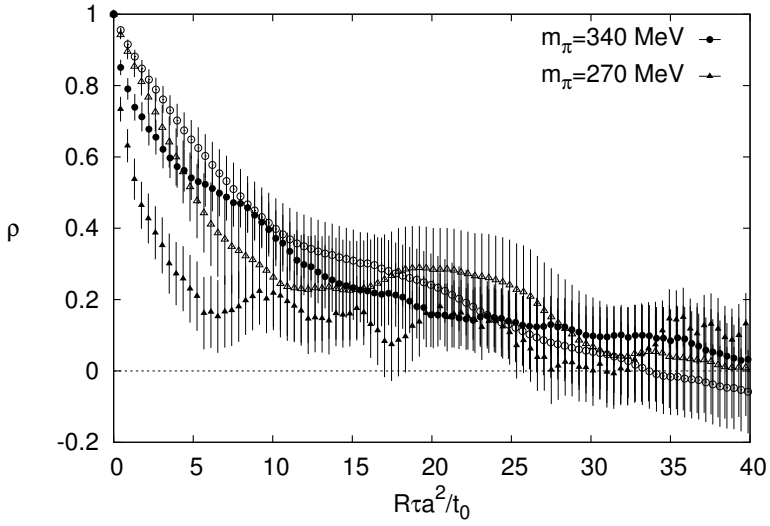

Figure 2. Autocorrelation function $\rho(\tau)$ at different pion masses for $\beta = 5.5$. For Q^2 (filled symbols) there is a clear suppression at smaller quark masses, whereas E (open symbols) does not show an effect beyond the statistical accuracy.

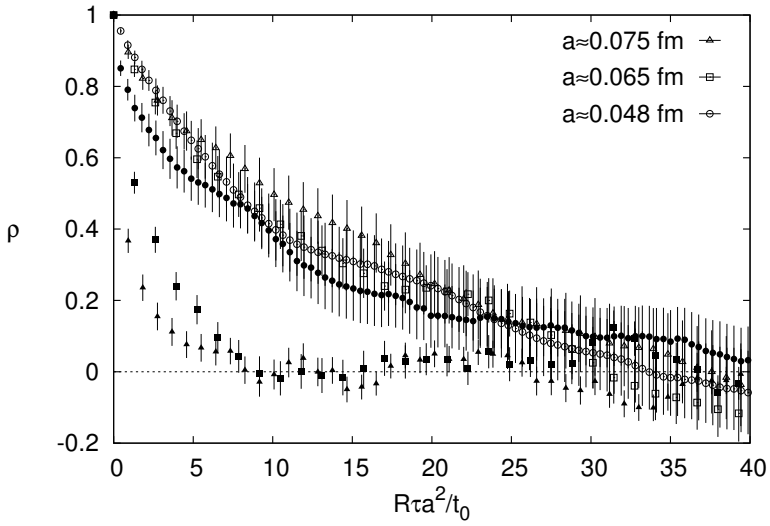

Figure 3. Autocorrelation function for different values of the lattice spacing. Open symbols correspond to E and filled to Q^2. ρ_E shows the expected scaling, whereas Q^2 is significantly faster on the coarser lattices.

JHEP08(2014)150

ID	$R\tau_{\rm int}(E)$	$R\tau_{\rm int}(Q^2)$
A2	55(22)	6(1)
A4	42(16)	5(1)
A5	49(18)	4(1)
B6	45(21)	4(1)
oB6	30(14)	—
E5g	47(15)	12(3)
F6	36(15)	10(3)
F7	83(35)	11(3)
G8	57(26)	4(1)
N6	105(38)	100(41)
O7	102(44)	52(21)

Table 2. Integrated autocorrelation times measured on our set of ensembles where sufficient statistics is available.

In an earlier publication [9], an estimate of $\tau_{\rm exp}(\beta)$ has been given based on the scaling of $\tau_{\rm int}(Q^2)$ in pure gauge theory normalized to the value of the E5 lattice. Since the topological charge is not the slowest quantity in this region, this is overly pessimistic for $\beta = 5.5$, where it gives twice the $\tau_{\rm int}(Q^2)$ observed and overly optimistic at $\beta = 5.2$.

Since the autocorrelations of the topological charge show a scaling compatible with what has been found in pure gauge theory, i.e. $\tau_{\rm int}(Q^2) \propto a^{-5}$, we expect that for our range of quark masses and $\beta > 5.5$ the charge will dominate the scaling of $\tau_{\rm exp}$.

2.3.1 Open boundary conditions

The use of open boundary conditions is expected to accelerate the sampling of the topological charge, which at fine lattice spacings is expected to be the slowest observable. However, we observe that this is not the case for our lattices, in particular at $\beta = 5.2$ where oB6 has been simulated. Here the bulk tunneling dominates over the effect of the open boundaries.

Within the accuracy of the result for $\tau_{\rm int}(E)$ reported in table 2, no advantage in terms of autocorrelations is visible between B6 and oB6. For this comparison, we compute the energy density on the time slices in $x_0/a \in [20, 171]$ in which the effect on the observable from the boundaries is negligible.

With open BC the notion of a global topological charge is lost, as will be discussed in the next section, therefore we do not compute $\tau_{\rm int}(Q^2)$ for oB6. For the alternative way to extract the susceptibility discussed below, we find comparable autocorrelation times for the two ensembles.

JHEP08(2014)150

3 Results

From the discussion in the previous section it should be clear that while we are confident that the statistics is sufficient for having control over the statistical errors, the accuracy of the susceptibility which can be reached from these ensembles only allows for qualitative statements. It is certainly not on par with the precision reached in pure gauge theory.

We will start by discussing the separation of topological sectors as the continuum is approached. In some sense, this is a measure for the physics associated with topology being realized already at a finite lattice spacing. It also is the reason for the Hybrid Monte Carlo algorithm having difficulty to decorrelate the topological charge.

Once this is established, we turn to the topological susceptibility, studying systematic effects between different ways of constructing it. This will be important for its determination imposing open boundary conditions in time, where the global topological charge is no longer a suitable observable.

3.1 Separation between the sectors

With periodic boundary conditions field space is disconnected in the continuum gauge theory. This property is obfuscated by ultra-violet fluctuations of the gauge fields and for a long time whether and in which way these sectors emerge as the lattice spacing decreases has been unclear. Using the smoothing provided by the Wilson flow, the emergence of the topological sectors in the continuum limit can finally be understood [10]. For convenience we here repeat the arguments in [10] in a rather explicit manner.

First one notices that it was shown long ago, that the space of lattice gauge fields U separates into disconnected sectors provided the gauge fields U are smooth enough, which means that

$$s_p(U) = \mathrm{Re}\,\mathrm{tr}\{1 - U(p)\} \tag{3.1}$$

satisfies

$$s_p(U) < s_{\mathrm{cut}} = 0.067\,, \tag{3.2}$$

for all plaquettes p on the lattice [30, 31].[3]

Secondly, the Wilson flow defines a map $U \equiv V_0 \leftrightarrow V_t$ of the gauge fields in our path integral to smoothed fields $V_t\,,\ t > 0$. Since this map is one-to-one, a classification of V_t in sectors is also one of the original fields U. Fields V_t are smooth since the total (global) action $S_{\mathrm{W}}(V) = \sum_p \frac{1}{g_0^2} s_p(V)$ is decreased by the flow, $S_{\mathrm{W}}(V_t) < S_{\mathrm{W}}(V_{t'})$ for $t > t'$. Of course, this does not mean that the local bound eq. (3.2) will be satisfied for V_t at a given t. However, if the number of plaquettes which violate $s_p(V_t) < s_{\mathrm{cut}}$ decreases strongly as one approaches $a \to 0$, we can say that sectors develop dynamically in the continuum limit.

Thirdly, in ref. [10] violations of the bound eq. (3.2) are investigated numerically using the probability that one plaquette violates the bound

$$P_t(s_{\mathrm{cut}}) = \frac{1}{6V}\langle \sum_p \theta(s_{\mathrm{cut}} - s_p(V_t))\rangle\,, \tag{3.3}$$

[3] For attempts to construct gauge actions which satisfy the bound automatically *and* can be used in numerical simulations, see [32] while for related questions of universality we refer to [33].

JHEP08(2014)150

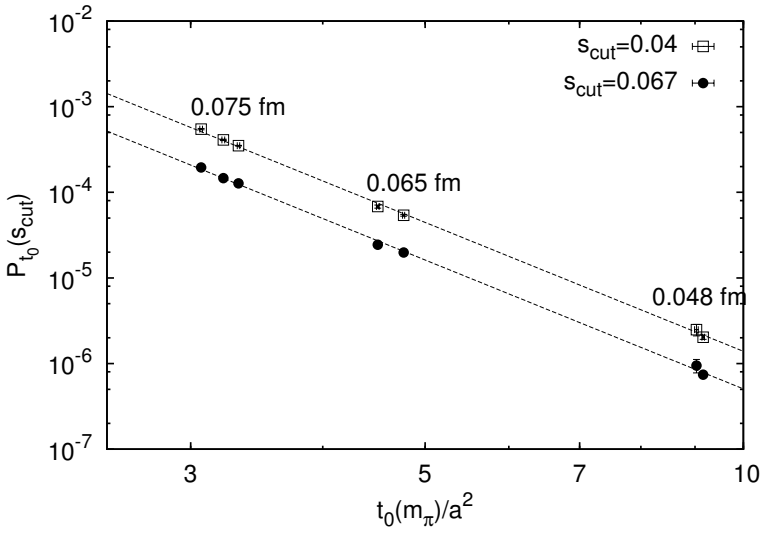

Figure 4. The probability $P_{t_0}(s_{\rm cut})$ of finding a plaquette value $s_p(V_t) \geq s_{\rm cut}$ as a function of the lattice spacing. The dotted lines represent a power law decay with $P_{t_0}(s_{\rm cut}) \propto a^{10}$.

It finds that in pure gauge theory with the Wilson action $P_t(s_{\rm cut}) \sim a^{10}$, which also suggests that in a fixed volume the probability for any plaquette violating the bound decreases as a^6.

As can be seen in figure 4, we find the same power law behavior in our two flavor simulations. While two values of $s_{\rm cut}$ are shown, the scaling does not depend significantly on $s_{\rm cut}$ in the investigated range up to $s_{\rm cut} = 0.1$ and the exponent is compatible with the pure gauge theory result of ref. [10]. It is remarkable that the effect of the quark mass on $P_{t_0}(s_{\rm cut})$ is completely compensated by its effect on t_0 and we observe universal scaling curves for each value of $s_{\rm cut}$. At a fixed β, smaller quark masses lead to a stronger separation of the sectors. In particular the presence of fermions does not alter the picture of ref. [10].

3.2 Computation of the topological susceptibility

With periodic boundary conditions for the gauge fields,

$$\chi^{\rm glob} = \frac{1}{V}\langle Q^2 \rangle \tag{3.4}$$

is the natural estimator for the topological susceptibility. With open boundary conditions in time, the same quantity would show large finite volume effects.[4] Therefore we rewrite eq. (1.2) restricting the time separation between the two densities to an upper bound r

$$\chi^{\rm corr}(r) = \frac{a^2}{TL^3} \sum_{z_0=0}^{T-1} \sum_{x_0=-r}^{r} \langle \bar{q}(z_0)\bar{q}(x_0+z_0)\rangle \quad ; \quad \bar{q}(x_0) = a^3 \sum_{\mathbf{x}} q(x_0,\mathbf{x})\,, \tag{3.5}$$

[4]With significant statistical uncertainties, ref. [34] does not resolve finite T effects in a comparision of $\chi_{\rm top}$ from open and periodic boundary conditions at flow time $t = t_0$. At smaller flow times, however, deviations are seen.

JHEP08(2014)150

ID	$t_1^2\chi^{\mathrm{glob}}_{t_0/2}$	$t_1^2\chi^{\mathrm{corr}}_{t_0/2}$	$t_0^2\chi^{\mathrm{corr}}_{t_0/2}$	$t_1^2\chi^{\mathrm{glob}}_{t_0}$	$t_1^2\chi^{\mathrm{glob}}_{t_1}$
A2	1.48(14)	1.46(11)	0.27(02)	1.67(17)	1.76(17)
A4	1.06(10)	1.10(08)	0.19(01)	1.21(12)	1.26(12)
A5	0.88(07)	0.97(06)	0.17(01)	0.94(07)	1.00(08)
B6	0.81(14)	0.81(08)	0.14(01)	0.90(15)	0.93(15)
oB6	—	—	0.15(02)	—	—
E5g	1.02(09)	1.09(09)	0.19(02)	1.08(10)	1.11(11)
F6	1.00(16)	0.93(09)	0.16(02)	1.04(17)	1.05(18)
F7	0.72(09)	0.71(08)	0.12(01)	0.78(10)	0.80(11)
G8	0.58(07)	0.75(10)	0.12(02)	0.60(09)	0.60(09)
N6	0.67(14)	0.72(15)	0.12(02)	0.68(14)	0.69(15)
O7	0.40(08)	0.47(13)	0.08(02)	0.41(08)	0.40(08)

Table 3. Results of the topological susceptibility from eq. (3.4), with Q measured also at $t = t_1$, and eq. (3.5). The scales t_0 and t_1 do always take the value at the finite quark mass of the corresponding ensemble. All the values have been multiplied by a factor 10^3. For most of the ensembles, χ^{corr} turns out to be more precise.

with $\chi^{\mathrm{corr}}(T/2-a)+\frac{a^2}{TL^3}\langle\bar{q}(0)\bar{q}(T/2)\rangle$ giving the full formula for periodic boundaries with even T/a. The correlator $\langle\bar{q}(z_0)\bar{q}(x_0+z_0)\rangle$ will be studied below. As we will see, it falls off quickly for large x_0 such that the sum can be truncated at moderate r.

To avoid finite T effects, in our case of open boundary conditions, all temporal arguments need to be sufficiently far away from the boundaries, i.e., x_0, $T-x_0$, x_0+z_0, $T-(x_0+z_0)$ need to be large in units of the inverse mass of the lightest state with vacuum quantum numbers.

In order to study the effect of the truncation in eq. (3.5), we plot the correlator between the slice charges for several values of the lattice spacings on the periodic lattices in the left panel of figure 5. This correlation function is positive for small distances, then turns negative and approaches zero for $x_0 \to \infty$. The sum over x_0 as a function of the upper bound is depicted on the right panel. As we can see, for our statistics a plateau is reached around $r/\sqrt{t_1} = 5$. This holds for all our ensembles. We therefore cut the summation at this point; the results are collected in table 3.

In these figures, it is interesting to note that while the large x_0 region shows almost perfect scaling, a significant cut-off effect is visible at $x_0 = 0$. Indeed, if this point is excluded from the summation in eq. (3.5), the sum does not show any scaling violation beyond its statistical accuracy.

In table 3 we also report the result of our ensemble with open BC, namely oB6. We observe that for this lattice spacing and pion mass the influence of the boundaries in $\langle\bar{q}(x_0)^2\rangle$ is visible with the present accuray up to 1.5 fm. Therefore, we restrict the computation of the susceptibility given in eq. (3.5) to time slices in the range $[20, 171]$; the summation window remains fixed to $r = 5\sqrt{t_1}$. No differences to B6 are observed in the final result

JHEP08(2014)150

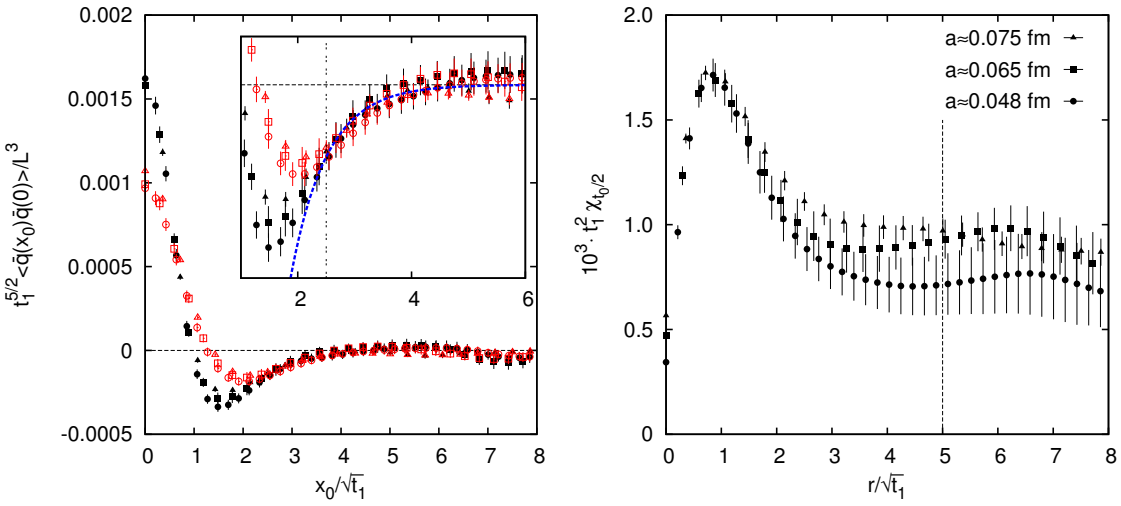

Figure 5. Determination of the susceptibility from the correlation function of the time slice summed charge at $t = t_0$ (open symbols) and $t = t_0/2$ (filled symbols); the scales t_0 and t_1 are taken at the quark mass of the ensemble. In both plots the ensembles are A5, F6 and N6. For the time-slice correlation functions in the left panel, the long distance behavior can be described by a single exponential decay as discussed in the text. In the right panel, the sum up to a window r is represented, with the vertical line the one used in our analysis.

and the errors are about the same. The reason is that the statistics is roughly the same. Furthermore, the reweighting factors of the twisted mass reweighting employed in the oB6 ensemble decouple almost completely from pure gluonic observables such as the charge.

3.2.1 Numerical estimate of the tail

We then fitted the correlation function to a single exponential as shown in figure 5, and estimated the systematic error of $\chi^{\mathrm{corr}}(r)$ from the integral over the fit function. As argued below this ansatz is justified in this situation despite the four-dimensional smoothing of the flow.

The fit was done to the data with $t = t_0/2$ shown in the figure, namely together to the data at the three values of a, neglecting scaling violations and in a range $2.5 \leq x_0\, t_1^{-1/2} \leq 6$. The thus determined systematic error turns out to be below 1%, much smaller than our statistical one. Even if our model underestimated the integral by a factor 4, which seems unlikely given the reasonable agreement with the data, the tail would still be negligible with our present accuracy.

3.2.2 Effects of the smoothing footprint in the large time behavior

The neglected tail gives a systematic error of this measurement. In order to justify the above estimate of its contribution, we need to be sure that the single exponential ansatz is expected to give a satisfactory description of the data in the range where it is applied.

The exponential decay with the mass of the flavor singlet pseudoscalar is modified due to two effects: the contribution of excited states and the fact that we apply a four

JHEP08(2014)150

dimensional smoothing to our observables. Since the flow generates a footprint of size $\sqrt{8t}$ with a Gaussian profile, one expects that for sufficiently large x_0 this modification is negligible. With a lowest mass m_0 in the considered channel, dimensional analysis leads one to expect that it can be neglected once $x_0/(8t\,m_0) \gg 1$.

To gain more insight into the influence of the smoothing on the shape of the two-point function, we consider the model of a free smoothed scalar field,

$$\Phi_t(x) \propto \int \mathrm{d}^4 z\, \mathrm{e}^{-(z-x)^2/(4t)} \Phi(z)\,, \tag{3.6}$$

noting that in lowest order of perturbation theory, the gluon field is smoothed in exactly the same way. Its time-slice correlation function at zero spatial momentum is given by

$$C_t(x_0) \equiv \int \mathrm{d}\,\mathbf{x}\, \langle \Phi_t(x) \Phi_t(0) \rangle \propto \int \mathrm{d}z_0\, \mathrm{e}^{-z_0^2/(8t) - m|z_0+x_0|}\,, \tag{3.7}$$

where m is the the mass of the scalar field. The large time asymptotics is given by

$$C_t(x_0) \propto \mathrm{e}^{-\mu\xi} \left(1 - \mathrm{e}^{-(\xi-\mu/2)^2} \left[\frac{\mu}{2\sqrt{\pi}\xi^2} + \mathrm{O}(\xi^{-4})\right]\right) \tag{3.8}$$

where we used dimensionless variables $\mu = \sqrt{8t}\,m$, $\xi = x_0/\sqrt{8t}$. The corrections to the asymptotic exponential decay due to the footprint of the smoothing are of order $\xi^{-2}\,\mathrm{e}^{-(\xi-\mu/2)^2}$. They are small once $\xi - \mu/2 > c$, or equivalently $x_0 > c\sqrt{8t} + 4tm$, and $c = 1.5$ or $c = 3$, with the effect of the smoothing in the per cent and far below the per mille range, respectively.

While our explicit computation is in a model, we believe that it provides a good general guideline. In particular the structure with the two different terms is expected to be a general feature.

For our case, the relevant mass is $m_0 \approx 1\,\mathrm{GeV}$. Choosing $t = t_0/2$, we have $\mu \approx 1.5$ and $\xi > 2$ translates into a footprint effect of less than 3%. Since the discussion in section 3.2.1 is about a systematic effect on the neglected tail, i.e., on a small systematic error itself, such an accuracy is more than sufficient in particular in view of our statistical uncertainties.

3.3 Distribution of the topological charge

In the large volume limit, the topological charge is expected to follow a Gaussian distribution, with the width given by the topological susceptibility. In figure 6 we show the cumulative distribution function $C(Q)$, which gives the probability of a configuration having charge smaller than Q, along with the measurement on three different ensembles. The theoretical lines use as width of the Gaussian distribution the measured value of χ^{corr} of table 3. The agreement with a Gaussian distribution is very reasonable, with only small deviations visible in the tails at $a = 0.048\,\mathrm{fm}$, which we attribute to our limited sampling of the tails.

3.4 Continuum limit and dependence on the light quark mass

In leading order in Chiral Perturbation Theory, the topological susceptibility is linear in the quark mass [17], or using the Gell-Mann-Oakes-Renner relation

$$\chi = \frac{m}{2}\Sigma\,(1 + O(m)) = \frac{1}{8} f_\pi^2 m_\pi^2 (1 + O(m_\pi^2))\,. \tag{3.9}$$

JHEP08(2014)150

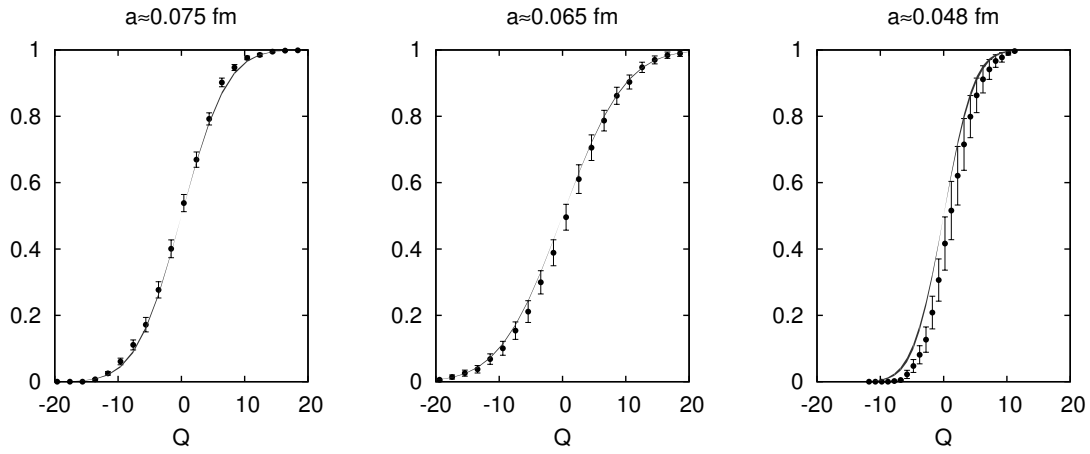

Figure 6. Plot of the cumulative distribution function of the topological charge for three ensembles. The solid lines represent a Gaussian distribution with the width coming from the measured topological susceptibility.

We therefore display the results for χ^{corr} from table 3 in figure 7 in terms of the dimensionless variable $t_1 m_\pi^2$, where we always take $t_1 = t_1(m_\pi)$, the value of the respective ensemble. With the lattice spacing determined from the kaon decay constant [27] and the pion decay constant set to 130.4 MeV, we obtain the line represented in the figure. Also shown is the pure gauge result of ref. [35].[5] The comparison confirms the strong effect of the presence of the fermions found in previous studies.

In the figure, a strong cut-off effect is visible, with the topological susceptibility significantly enhanced for the coarser lattices. Because of the breaking of chiral symmetry, at finite lattice spacing there is no reason for the susceptibility to vanish at vanishing pion mass. Assuming leading effects of $\mathrm{O}(a^2)$, Wilson Chiral Perturbation Theory suggests the following ansatz[6]

$$t_1^2 \chi_{\mathrm{top}} = c\, t_1\, m_\pi^2 + a^2 \frac{b}{t_1}\,. \tag{3.10}$$

The result is also shown in figure 7. As can be seen, the description of the data is satisfactory given the large error bands and the continuum limit is compatible with the LO ChPT expectation. We find for the slope $c = 2.8(5) \cdot 10^{-3}$, for the intercept $b = 5.1(7) \cdot 10^{-3}$ and a χ^2/d.o.f of the global fit of 1.17.

4 Conclusions

Measurements of observables with long autocorrelation times are difficult and the topological susceptibility is no exception. However, we found that for the action used in the CLS simulation, the topological charge is not yet the slowest observable in the range of lattice

[5] Despite the lower statistical accuracy, we prefer this result to others obtained with smearing and cooling because the definition via the index of a chirally symmetric Dirac operator has a well-defined continuum limit.

[6] We are indebted to Oliver Bär for communicating unpublished results regarding this issue.

JHEP08(2014)150

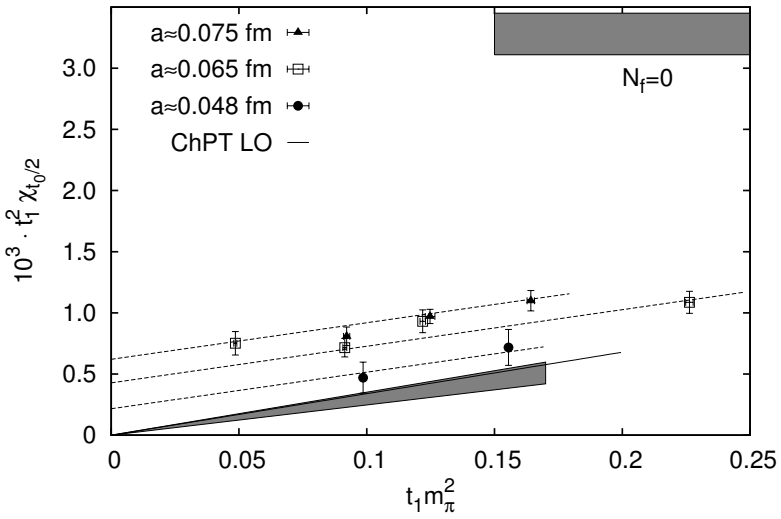

Figure 7. The values of the topological susceptibility χ^{corr} from table 3 along with the leading order expectation from ChPT and the pure gauge value.

spacings under investigation, though the rapid growth in τ_{int} indicates that on slightly finer lattices the charge would effectively freeze in typical simulations. We show that light quarks mitigate the problem of the slow topological charge to a certain extent, whereas the other slow modes, as seen, e.g., in $E(t_0)$, do not profit.

Larger quark masses and also cut-off effects (for the action employed in this paper) both increase the susceptibility, however, even on our coarsest lattices and largest pion mass of 630 MeV, we observe a suppression of the susceptibility with respect to the pure gauge case by more than 50%. The three lattice spacings with a range of pion masses at our disposal allow us to take the continuum limit with theoretical support from Wilson Chiral Perturbation Theory. As we have shown, for fitting the pion mass dependence of χ_{top} at finite lattice spacing, it is crucial to include a term that does not vanish at zero pion mass and finite cutoff. Only with chirally symmetric sea quarks such a term can be excluded.

We stress that discretization effects seem large, because the quantity of interest is small for small quark masses. In such a situation, large relative discretization errors are generic, however, the scale to judge them is the deviation from the pure gauge theory result and on this scale we reach a percent level accuracy in the continuum for the whole quark mass region.

Finally let us point out that the discussion in section 3.2.2 on the effects of the footprint is particularly relevant when one wants to extract masses from correlation functions at positive flow time. For example the glueball mass determination using the method suggested in ref. [36] may be affected.

JHEP08(2014)150

Acknowledgments

We thank Francesco Virotta for collaboration in an early stage of this project. It is also a pleasure to thank Oliver Bär for essential discussion concerning the Wilson Chiral Perturbation Theory prediction and Stefan Sint and Ulli Wolff for discussion. This project used $N_f = 2$ gauge field configurations generated within the CLS effort; we are grateful to our colleagues for sharing them with us. We thankfully acknowledge the computer resources granted by the John von Neumann Institute for Computing (NIC) and provided on the supercomputer JUROPA at Jülich Supercomputing Centre (JSC) and by the Gauss Centre for Supercomputing (GCS) through the NIC on the GCS share of the supercomputer JUQUEEN at JSC, with funding by the German Federal Ministry of Education and Research (BMBF) and the German State Ministries for Research of Baden-Württemberg (MWK), Bayern (StMWFK) and Nordrhein-Westfalen (MIWF), as well as within the Distributed European Computing Initiative by the PRACE-2IP, with funding from the European Community's Seventh Framework Programme (FP7/2007-2013) under grant agreement RI-283493, by the HLRN in Berlin, and by NIC at DESY, Zeuthen.

References

[1] E. Witten, *Current algebra theorems for the* U(1) *Goldstone boson*, *Nucl. Phys.* **B 156** (1979) 269 [INSPIRE].

[2] G. Veneziano, U(1) *without instantons*, *Nucl. Phys.* **B 159** (1979) 213 [INSPIRE].

[3] P. Hasenfratz, V. Laliena and F. Niedermayer, *The index theorem in QCD with a finite cutoff*, *Phys. Lett.* **B 427** (1998) 125 [hep-lat/9801021] [INSPIRE].

[4] L. Giusti, G.C. Rossi, M. Testa and G. Veneziano, *The* $U_A(1)$ *problem on the lattice with Ginsparg-Wilson fermions*, *Nucl. Phys.* **B 628** (2002) 234 [hep-lat/0108009] [INSPIRE].

[5] L. Giusti, G.C. Rossi and M. Testa, *Topological susceptibility in full QCD with Ginsparg-Wilson fermions*, *Phys. Lett.* **B 587** (2004) 157 [hep-lat/0402027] [INSPIRE].

[6] M. Lüscher, *Topological effects in QCD and the problem of short distance singularities*, *Phys. Lett.* **B 593** (2004) 296 [hep-th/0404034] [INSPIRE].

[7] M. Lüscher, *Properties and uses of the Wilson flow in lattice QCD*, *JHEP* **08** (2010) 071 [arXiv:1006.4518] [INSPIRE].

[8] M. Lüscher and F. Palombi, *Universality of the topological susceptibility in the* SU(3) *gauge theory*, *JHEP* **09** (2010) 110 [arXiv:1008.0732] [INSPIRE].

[9] ALPHA collaboration, S. Schaefer, R. Sommer and F. Virotta, *Critical slowing down and error analysis in lattice QCD simulations*, *Nucl. Phys.* **B 845** (2011) 93 [arXiv:1009.5228] [INSPIRE].

[10] M. Lüscher, *Topology, the Wilson flow and the HMC algorithm*, PoS(LATTICE 2010)015 [arXiv:1009.5877] [INSPIRE].

JHEP08(2014)150

[11] M. Lüscher and S. Schaefer, *Lattice QCD without topology barriers*, *JHEP* **07** (2011) 036 [arXiv:1105.4749] [INSPIRE].

[12] SESAM and T(X)L collaborations, G.S. Bali et al., *Quark mass effects on the topological susceptibility in QCD*, *Phys. Rev.* **D 64** (2001) 054502 [hep-lat/0102002] [INSPIRE].

[13] UKQCD collaboration, A. Hart and M. Teper, *The topological susceptibility and f_π from lattice QCD*, *Phys. Lett.* **B 523** (2001) 280 [hep-lat/0108006] [INSPIRE].

[14] QCDSF collaboration, A. Hart, *Discretization effects in the topological susceptibility in lattice QCD*, *Phys. Rev.* **D 69** (2004) 074510 [hep-lat/0401015] [INSPIRE].

[15] C. Bernard et al., *Topological susceptibility with the improved Asqtad action*, *Phys. Rev.* **D 68** (2003) 114501 [hep-lat/0308019] [INSPIRE].

[16] MILC collaboration, A. Bazavov et al., *Topological susceptibility with the Asqtad action*, *Phys. Rev.* **D 81** (2010) 114501 [arXiv:1003.5695] [INSPIRE].

[17] H. Leutwyler and A.V. Smilga, *Spectrum of Dirac operator and role of winding number in QCD*, *Phys. Rev.* **D 46** (1992) 5607 [INSPIRE].

[18] ETM collaboration, K. Cichy, E. Garcia-Ramos and K. Jansen, *Topological susceptibility from the twisted mass Dirac operator spectrum*, *JHEP* **02** (2014) 119 [arXiv:1312.5161] [INSPIRE].

[19] T.W. Chiu, T.H. Hsieh and Y.Y. Mao, *Topological susceptibility in two flavors lattice QCD with the optimal domain-wall fermion*, *Phys. Lett.* **B 702** (2011) 131 [arXiv:1105.4414] [INSPIRE].

[20] R. Sommer, *Scale setting in lattice QCD*, PoS(LATTICE 2013)015 [arXiv:1401.3270] [INSPIRE].

[21] M. Bruno and R. Sommer, *On the N_f-dependence of gluonic observables*, PoS(LATTICE 2013)321 [arXiv:1311.5585] [INSPIRE].

[22] S. Lottini, *Chiral behaviour of the pion decay constant in $N_f = 2$ QCD*, PoS(LATTICE 2013)315 [arXiv:1311.3081] [INSPIRE].

[23] M. Lüscher, *Schwarz-preconditioned HMC algorithm for two-flavour lattice QCD*, *Comput. Phys. Commun.* **165** (2005) 199 [hep-lat/0409106] [INSPIRE].

[24] M. Hasenbusch, *Speeding up the hybrid Monte Carlo algorithm for dynamical fermions*, *Phys. Lett.* **B 519** (2001) 177 [hep-lat/0107019] [INSPIRE].

[25] M. Marinkovic and S. Schaefer, *Comparison of the mass preconditioned HMC and the DD-HMC algorithm for two-flavour QCD*, PoS(LATTICE 2010)031 [arXiv:1011.0911] [INSPIRE].

[26] M. Lüscher and S. Schaefer, *Lattice QCD with open boundary conditions and twisted-mass reweighting*, *Comput. Phys. Commun.* **184** (2013) 519 [arXiv:1206.2809] [INSPIRE].

[27] P. Fritzsch et al., *The strange quark mass and Lambda parameter of two flavor QCD*, *Nucl. Phys.* **B 865** (2012) 397 [arXiv:1205.5380] [INSPIRE].

[28] M. Lüscher and S. Schaefer, *Non-renormalizability of the HMC algorithm*, *JHEP* **04** (2011) 104 [arXiv:1103.1810] [INSPIRE].

[29] A. Chowdhury et al., *Exploring autocorrelations in two-flavour Wilson lattice QCD using DD-HMC algorithm*, *Comput. Phys. Commun.* **184** (2013) 1439 [arXiv:1209.3915] [INSPIRE].

JHEP08(2014)150

[30] A. Phillips and D. Stone, *Lattice gauge fields, principal bundles and the calculation of topological charge*, *Commun. Math. Phys.* **103** (1986) 599 [INSPIRE].

[31] M. Lüscher, *Topology of lattice gauge fields*, *Commun. Math. Phys.* **85** (1982) 39 [INSPIRE].

[32] W. Bietenholz et al., *Exploring topology conserving gauge actions for lattice QCD*, *JHEP* **03** (2006) 017 [hep-lat/0511016] [INSPIRE].

[33] W. Bietenholz, U. Gerber, M. Pepe and U.-J. Wiese, *Topological lattice actions*, *JHEP* **12** (2010) 020 [arXiv:1009.2146] [INSPIRE].

[34] A. Chowdhury, A. Harindranath, J. Maiti and P. Majumdar, *Topological susceptibility in lattice Yang-Mills theory with open boundary condition*, *JHEP* **02** (2014) 045 [arXiv:1311.6599] [INSPIRE].

[35] L. Del Debbio, L. Giusti and C. Pica, *Topological susceptibility in the* SU(3) *gauge theory*, *Phys. Rev. Lett.* **94** (2005) 032003 [hep-th/0407052] [INSPIRE].

[36] A. Chowdhury, A. Harindranath and J. Maiti, *Open boundary condition, Wilson flow and the scalar glueball mass*, *JHEP* **06** (2014) 067 [arXiv:1402.7138] [INSPIRE].

JHEP08(2014)150